

Interaction between two hadrons in lattice QCD

Sinya Aoki^{a,*}

^a*Center for Gravitational Physics and Quantum Information, Yukawa Institute for Theoretical Physics, Kyoto University, Kitashirakawa Oiwakecho, Sakyo-ku, Kyoto 606-8502, Japan*

E-mail: saoki@yukawa.kyoto-u.ac.jp

I report recent developments on hadron interactions in lattice QCD by the HAL QCD method. As an introduction, I summarize the lattice community's consensus on the absence of the deeply bound dinucleons at heavier pion masses. We then present 4 results by the HAL QCD method using 2 + 1 flavor QCD gauge configurations at $m_\pi \simeq 146$ MeV and $a \simeq 0.0846$ fm, which are the $\Lambda\Lambda - N\Xi$ interactions, $N\Omega$ dibaryon, the tetra-quark state T_{cc} and the $N - \phi$ interaction with the 2-pion tail. A brief summary follows.

*The 11th International Workshop on Chiral Dynamics (CD2024)
26-30 August 2024
Ruhr University Bochum, Germany*

*Speaker

1. Introduction

In lattice QCD, there are two methods utilized to extract interactions between hadrons, one is the finite volume (FV) method, which extracts scattering phase shifts from spectra of two hadrons in finite boxes through Lüscher’s finite volume formula[1], the other is the HAL QCD method, which first extracts a potential (interaction kernel) from the NBS (Nambu-Bethe-Salpeter) wave function and then obtains scattering phase shifts by solving Schrödinger equation with the potential[2–4].

It is always better to have two different methods for crosschecks. Indeed, in the past, there appeared so called “the NN controversy” in the community: While the FV method claimed that both deuteron and dineutron are bound at heavier pion masses[5–9], the HAL QCD potential method found that both are unbound there[10, 11].

Since then, there appeared more results using the FV method from the community to resolve this controversy. At lattice 2023, Walker-Loud[12] categorized all results known at that time into two groups, (A) deeply bound dinucleons or (B) no bound state. This classification shows that the controversy is not caused by the difference of methods, the FV method or the HAL QCD method. Instead he pointed out that results with deeply bound dinucleons were obtained from FV spectra with compact hexa-quark source operators[5–9] but results with no bound dinucleons comes from calculations with diffuse sources such as wall sources (HAL QCD)[10, 11], distillation (Mainz)[13], stochastic LapH (CoSMoN)[14] or sparsening momentum (NPLQCD)[15].

A comparative study on FV spectra between the wall source and the hexa-quark source has suggested that the hexa-quark source tends to create a fake plateau for correlation functions of dinucleons, which can be misidentified as “a deeply bound state”[16, 17]. The HAL QCD collaboration performed a extensive study[18] and found that a naive plateau identification employed by old studies in the FV method cannot control systematics from excited state contaminations, while the HAL QCD method does not suffer from this issue. It was also explicitly shown that the plateaux from the hexa-quark source are indeed fake. By addressing this issue using optimized (sink) operators, the HAL QCD collaboration showed that the results from the FV method become consistent with those from the HAL QCD method, i.e., unbound NN systems. New calculations by the more sophisticated FV method followed. At lattice 2022, Nicholson[19] presented Fig. 1(Left), which compares $q \cot \delta(q)/m_\pi$ as a function of q^2/m_π^2 among the HAL QCD method at $m_\pi \simeq 715$ MeV (purple band) and the FV method with the diffused source at $m_\pi \simeq 715$ MeV (red, blue and magenta symbols) and the hexa-quark source at $m_\pi \simeq 800$ MeV (green squares), where $\delta(q)$ is the scattering phase shift of $NN(^3S_1)$. The first two are consistent with each other, showing the absence of the bound deuteron, while the last one is totally different in behaviors of $q \cot \delta(q)$, which intersects the bound state condition (cyan line) giving the deeply bound deuteron.¹ Now the community’s consensus is that old FV results with hexa-quark sources have large uncertainties on the extraction of FV spectra, due to the fake plateau problem, as summarized in the statement by Walker-Loud at lattice 2023[12] that “I believe the old results are wrong (including those I was involved with)”. Two nucleons are unbound at heavier pion masses. Since results claiming bound three or more baryons also employed the hexa-quark sources[5, 6], they are unreliable, too, so are

¹A combination of the FV formula and the effective range expansion of $q \cot \delta(q)$ was first introduced by the HAL QCD collaboration to check a normality of the bound stat spectra in the finite box[17].

matrix element calculations of such “bound states” (for example, Re. [20]). See also plenary talks by Morningstar and Green[21] in this conference (CD2024).

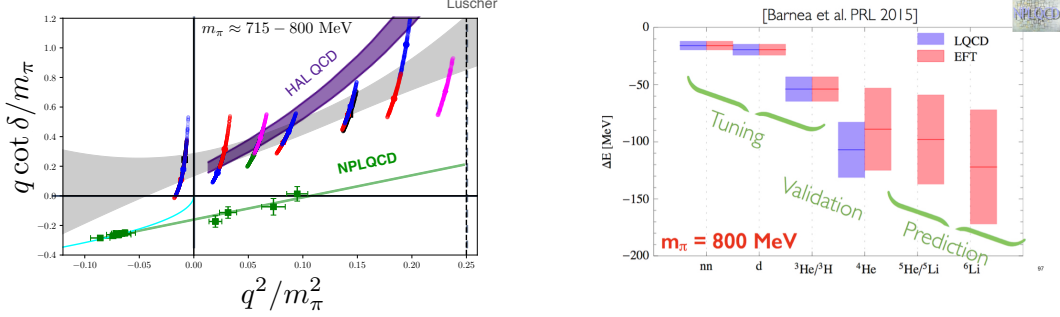


Figure 1: (Left) The $q \cot \delta(q)/m_\pi$ as a function of q^2/m_π^2 for the NN scattering in the 3S_1 channel, obtained by the FV method with the diffused source at $m_\pi \approx 715$ MeV (red, blue and magenta symbols) and the hexa-quark source at $m_\pi \approx 800$ MeV (green squares), together with the one by the HAL QCD method on the same configurations at $m_\pi \approx 715$ MeV (purple band). Figure taken from the slide by Nicholson at lattice 2022[19]. (Right) A comparison of binding energies between the lattice QCD at $m_\pi = 800$ MeV[6] (blue) and the pionless EFT (red). Deuteron, dineutron and $^3\text{He}/^3\text{H}$ are used to fix low energy constants of the pionless EFT, while ^4He is used to validate the fixed low energy constants. Then the pionless EFT predicts binding energies of $^5\text{He}/^5\text{Li}$ and ^6Li . Figure taken from the slide by Beane at CD2015[22].

Could (chiral) effective theories invalidate old FV data ? Unfortunately, the answer is “No”. Beane made Fig. 1(Right) at CD2015[22] using the data in Ref. [23], to claim that the pionless EFT, by fixing its low energy constants from the old lattice result in the FV method[6] on binding energies of deuteron, dineutron and $^3\text{He}/^3\text{H}$ at $m_\pi = 800$ MeV, validates the lattice data on the binding energy of ^4He at the same pion mass. Similarly, the chiral perturbation theory predicted pion mass dependences of binding energy and momentum, which reasonably agree with the old lattice data in the FV method at four pion masses above 300 MeV[24]. (See, however, the chiral EFT analysis which found inconsistency within old lattice data in the FV method[25].) It seems that the chiral effective theories can tell consistencies among lattice data but cannot check correctness of lattice data themselves.

In this talk, I will review recent results on interactions between two hadrons at almost physical pion mass, obtained exclusively by the HAL QCD method, emphasizing connections with chiral dynamics or experimental data.

2. HAL QCD method

We here briefly introduce the coupled channel HAL QCD method. The coupled channel potential is extracted by the time-dependent HAL QCD method as

$$\left(\frac{1 + 3\delta_c^2}{8\mu_c} \frac{\partial^2}{\partial t^2} - \frac{\partial}{\partial t} + \frac{\nabla^2}{2\mu_c} \right) R^c_d(\vec{r}, t) = \sum_{c'} \int d^3r' U^c_{c'}(\vec{r}, \vec{r}') \Delta^c_{c'} R^{c'}_d(\vec{r}', t), \quad (1)$$

where c, d represent channel indices, and the correlation function matrix for two hadrons is defined by

$$R^c_d(\vec{r}, t) := \frac{\sum_{\vec{x}} \langle 0 | H_{c_1}(\vec{r} + \vec{x}, t) H_{c_1}(\vec{x}, t) \overline{\mathcal{J}}_d(0) | 0 \rangle}{\sqrt{Z_{c_1}} \sqrt{Z_{c_2}} \exp[-(m_{c_1} + m_{c_2})t]}. \quad (2)$$

Here H_{c_1} and H_{c_2} are local interpolating operators for hadrons while $\overline{\mathcal{J}}_d(0)$ is a source operator creating two hadrons at $t = 0$, and Z_{c_1} and Z_{c_2} denote wave function renormalization factors for each hadron. We also define the reduced mass $\mu_c = m_{c_1} m_{c_2} / (m_{c_1} + m_{c_2})$, the size of mass difference $\delta_c = (m_{c_1} - m_{c_2}) / (m_{c_1} + m_{c_2})$, the factor $\Delta^c_d = \exp[-(m_{d_1} + m_{d_2} - m_{c_1} - m_{c_2})t]$, which compensates the threshold energy difference between c and d channels.

In practice, the non-local potential $U^c_{c'}$ is treated in the derivative expansion as

$$U^c_{c'}(\vec{r}, \vec{r}') = \left(V^c_{c'}(\vec{r}) + \sum_{n=1} V^{(n)c}_{c'}(\vec{r}) \nabla^n \right) \delta(\vec{r} - \vec{r}'), \quad (3)$$

and employ the leading order (LO) potential $V^c_{c'}$ to obtain observables such as scattering phase shifts. Systematic errors associated with the LO truncation of the derivative expansion is estimated from t dependences of potentials and physical observables, which should be insensitive to sufficiently large t if higher order contributions are small.

All results in this talks have been obtained with gauges configurations on 96^4 lattice at almost physical pion mass, generated on the K-computer in Japan by the 2+1 flavor QCD with Iwasaki gauge action plus non-perturbatively $O(a)$ improved clover quark action at $a^{-1} \simeq 0.0846$ fm, so that the spatial extension $La \simeq 8.1$ fm is larger enough[26]. Some hadrons masses on this ensemble are $m_\pi \simeq 146$ MeV, $m_K \simeq 525$ MeV, $m_N \simeq 955$ MeV, $m_\phi \simeq 1048$ MeV, $m_\Lambda \simeq 1140$ MeV, $m_\Sigma \simeq 1222$ MeV, $m_\Xi \simeq 1355$ MeV and $m_\Omega \simeq 1712$ MeV.

3. $\Lambda\Lambda - N\Xi$ interactions

3.1 Lattice results at almost physical pion mass

In previous studies by the HAL QCD collaboration[11, 27, 28], the H dibaryon ($uuddss$ state) has appeared as a bound state at heavy pion mass in the flavor SU(3) limit ($m_u = m_d = m_s$). It has been observed that the binding energy decreases while a size of the bound state increases as the pion mass decreases. What happens in real world, where the pion mass becomes much lighter and the flavor SU(3) is violated? Three thresholds appear in the H dibaryon channel at $2m_\Lambda \simeq 2280$ MeV, $m_N + m_\Xi \simeq 2311$ MeV and $2m_\Sigma \simeq 2444$ MeV. We have calculated the $\Lambda\Lambda - N\Xi$ coupled channel interaction at almost physical pion mass, ignoring the $\Sigma\Sigma$ channel as its threshold is much higher.

In Fig. 2, we present the S -wave $\Lambda\Lambda - N\Xi$ coupled channel potentials in the $^{11}S_0$ channel obtained at almost physical pion mass, where we use the notation $^{2I+1, 2s+1}S_J$ to specify the total isospin I , total spin s and the total angular momentum J of S -wave states. First of all, t dependences of potentials are small, showing that the LO truncation of the derivative expansion is reasonably good. Off-diagonal potentials are non-zero only at short distance, indicating that the channel mixing between $\Lambda\Lambda$ and $N\Xi$ is negligible at low energies. Within diagonal potentials, the attraction in the $N\Xi$ channel is much stronger than $\Lambda\Lambda$. This tendency was observed already at heavier pion masses.

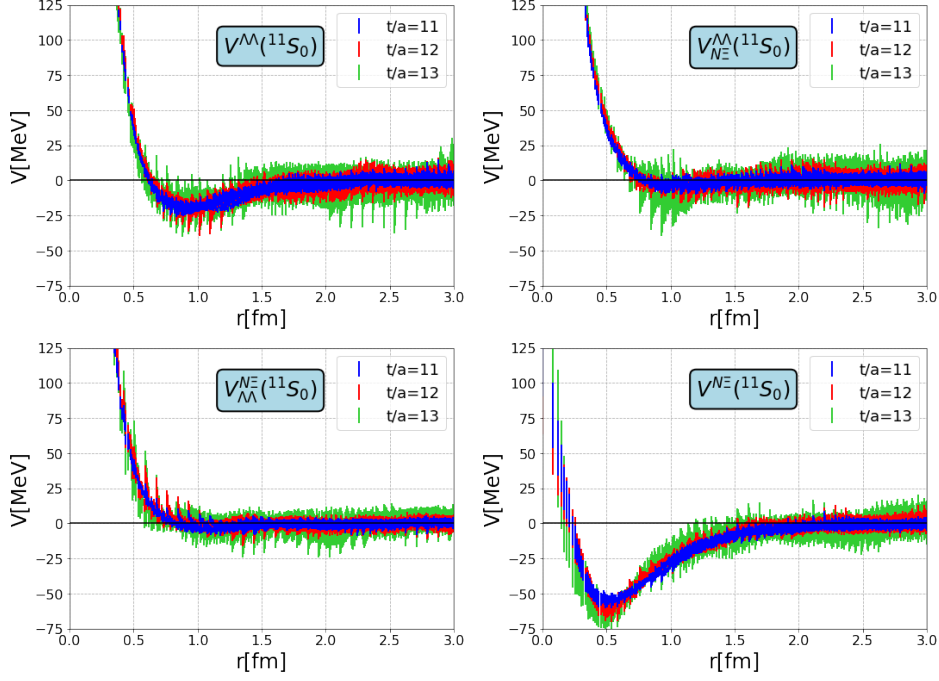


Figure 2: The S -wave $\Lambda\Lambda - N\Xi$ couple channel potentials in the 1S_0 as a function of the relative distance r . Here $V^{\Lambda\Lambda}$ (Upper-Left), $V_{N\Xi}^{\Lambda\Lambda}$ (Upper-Right), $V_{\Lambda\Lambda}^{N\Xi}$ (Lower-Left) and $V^{N\Xi}$ (Lower-Right) stand for $\Lambda\Lambda \rightarrow \Lambda\Lambda$ (diagonal), $N\Xi \rightarrow \Lambda\Lambda$ (off-diagonal), $\Lambda\Lambda \rightarrow N\Xi$ (off-diagonal) and $N\Xi \rightarrow N\Xi$ (diagonal), respectively. Figures taken from Ref. [29].

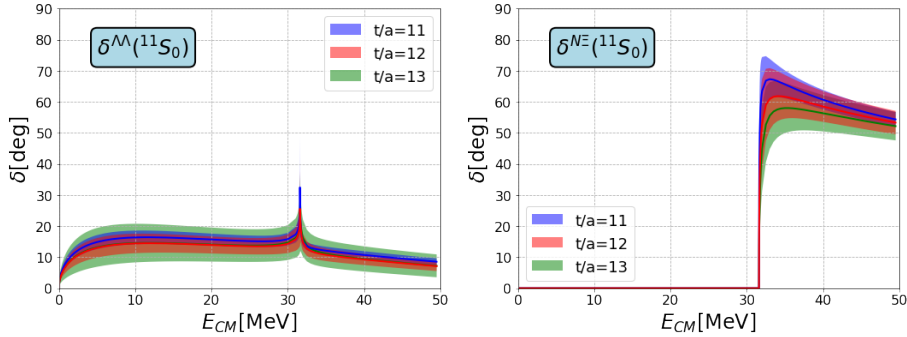


Figure 3: (Left) $\Lambda\Lambda$ scattering phase shift and (Right) $N\Xi$ scattering phase shift in the 1S_0 channel as a function of the center of mass energy E_{CM} from the $\Lambda\Lambda$ threshold. Figures taken from Ref. [29].

Fig. 3 shows scattering phase shifts of $\Lambda\Lambda$ (Left) and $N\Xi$ (Right) as a function of the center of mass energy E_{CM} from the $\Lambda\Lambda$ threshold[29]. A positive but small $\Lambda\Lambda$ scattering phase shift indicates that neither bound state nor resonance exists in this channel because of weak attraction in the diagonal $\Lambda\Lambda$ potential. In particular, no H dibaryon appears near the $\Lambda\Lambda$ threshold and we obtain $a_0^{\Lambda\Lambda} = 0.8(3)$ fm for the $\Lambda\Lambda$ scattering length. We observe a sharp enhancement and rapid drop of the $\Lambda\Lambda$ scattering phase shift near the $N\Xi$ threshold, which is caused by the off-diagonal potential between $\Lambda\Lambda$ and $N\Xi$. The $N\Xi$ scattering, on the other hand, exhibits a sharp increase near the $N\Xi$ threshold due to the significant attraction of the diagonal $N\Xi$ potential, whose maximum almost

reaches to 60 degrees. An analysis of the coupled channel scattering S-matrix in complex energy planes reveals that H dibaryon appears as a nearly virtual state with very small width near the $N\Xi$ threshold at $m_\pi \simeq 146$ MeV and $a \simeq 0.0846$ fm.

3.2 Comparison with experiments

RHIC and LHC have measured two hadron correlations, $C_{AB}(Q) = N_{AB}^{\text{pair}}(Q)/N_A(Q)N_B(Q)$, where $N_{AB}(Q)$ is a number of pairs of hadron A and hadron B in the final states of heavy ion collisions at energy Q , while $N_A(Q)$ and $N_B(Q)$ are those of the single hadron. One can estimate $N_{AB}(Q)$ as

$$N_{AB}(Q) = \int \frac{d^3 p_A}{E_A} \frac{d^3 p_B}{E_B} N_{AB}(\vec{p}_A, \vec{p}_B) \delta\left(Q - \sqrt{-q^2}\right), \quad q^2 = q_\mu q^\mu, \quad (4)$$

where q^μ is the relative 4 momentum, and

$$N_{AB}(\vec{p}_A, \vec{p}_B) \simeq \int d^4 x d^4 y S_{AB}(x, \vec{p}_A) S_B(y, \vec{p}_B) |\Psi(x, y, \vec{p}_A, \vec{p}_B)|^2. \quad (5)$$

Here S_A and S_B are source functions of each hadron and $\Psi(x, y, \vec{p}_A, \vec{p}_B)$ is the 2-body wave function between A and B , obtained from a solution to the Schrödinger equation with a given potential. Therefore, if source functions are approximately known, one can test hadron interactions against two hadron correlations obtained in experimental through the above formula, and vice versa. This type of analysis for hadron interactions through heavy ion collision experiments is called ‘‘Femtoscopy’’[30].

Fig. 4 (Upper) shows a comparison of hadron correlations between p (proton) and Ξ^- , where black symbols represent experimental data obtained at LHC by ALICE Collaboration [31] while pink and green bands give theoretical predictions by Coulomb with and without HALQCD interactions, respectively. As seen in the figure, the correlation obtained by the Coulomb with HALQCD potential agrees with the experimental data much better than the one by the Coulomb potential alone.

4. $N\Omega$ dibaryon

The $N\Omega$ potential in the 5S_2 channel ($s = 2$ and $J = 2$) has been calculated at almost physical pion mass, as shown in Fig. 5 (Left), which is attractive at all distances without repulsive core. This behavior is qualitatively the same at $m_\pi \simeq 875$ MeV[33]. At $m_\pi \simeq 146$ MeV, there are two thresholds, $\Lambda\Xi({}^{31}D_2)$ and $\Sigma\Xi({}^{31}D_2)$, below the $N\Omega({}^5S_2)$ threshold $E_{\text{th}}^{N\Omega} \simeq 2666$ MeV. Explicitly $E_{\text{th}}^{\Lambda\Xi({}^{31}D_2)} \simeq 2495$ (2514) MeV and $E_{\text{th}}^{\Sigma\Xi({}^{31}D_2)} \simeq 2577$ (2595) MeV at $L = \infty$ (8.1 fm) with L being the spacial extension. However only the single channel analysis was made in Ref. [33] by assuming small couplings to D -wave states, which is supported by the weak t dependence of the potentials. In future, the coupled channel analysis will be needed to check the current result.

Fig. 5 (Right) gives the $k \cot \delta_0(k)$ with $\delta_0(k)$ being the S -wave scattering phase shift, whose ERE fit leads to the scattering length $a_0 = -5.30(0.44)_{(-0.01)}^{(+0.16)}$ fm and the effective range $r_{\text{eff}} = 1.60(0.01)_{(-0.01)}^{(+0.02)}$ fm, where the central value and the statistical errors are estimated at $t/a = 12$ while the systematic errors in the last parentheses are estimated from the largest differences of the central values ($t/a = 12$) among $t/a = 11, 13, 14$. The behavior of the $k \cot \delta_0(k)$ suggests

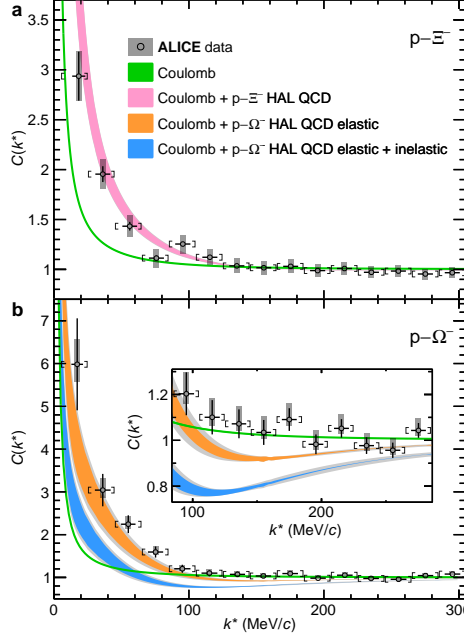


Figure 4: (Upper) Correlations between p (proton) and Ξ^- as a function of $k^* = |\vec{k}^*|$ with the relative momentum $\vec{k}^* = \vec{p}_A - \vec{p}_B$, where experimental data[31] are shown as black symbols while theoretical predictions by Coulomb with or without strong HALQCD interactions[29] are pink or green bands, respectively. (Lower) Correlations between p and Ω^- , where experimental data[31] are shown as black symbols while theoretical predictions by Coulomb, including HALQCD elastic interactions[32] or including both elastic & inelastic interactions are green, orange or blue bands, respectively. Figures taken from Ref. [31].

an existence of a bound state in this channel. A solution of the Schrödinger equation with the potential gives the binding energy $B = 1.54(0.30)^{(+0.04)}_{(-0.10)}$ MeV and the root mean square distance $\sqrt{\langle r^2 \rangle} = 3.77(0.31)^{(+0.11)}_{(-0.01)}$ fm. This binding energy is much smaller than $B = 18.9(5.0)^{(+12.1)}_{(-1.8)}$ MeV obtained at $m_\pi \simeq 875$ MeV[33]. The smallness of the binding energy at $m_\pi \simeq 146$ MeV is caused by the short range nature of the potential, though it is attractive everywhere. As the pion mass decreases, smaller masses of N and Ω increase the kinetic energy of the system, so that it is loosely bound like the deuteron and the root mean square distance becomes larger. If an extra attraction in the $p\Omega^-$ system due to the Coulomb interaction is included by adding $-\alpha/r$ term to the potential with $\alpha := e^2/(4\pi) = 1/137.036$, we obtain $B_{p\Omega^-} = 2.46(0.34)^{(+0.04)}_{(-0.11)}$ MeV and $\sqrt{\langle r^2 \rangle}_{p\Omega^-} = 3.24(0.19)^{(+0.06)}_{(-0.00)}$ fm.

Fig. 4 (Lower) shows a comparison of hadron correlations between p and Ω^- , where black symbols represent experimental data obtained by ALICE Collaboration[31] while green, orange or blue bands give theoretical predictions by Coulomb only, including HALQCD elastic in Fig. 5 or further adding inelastic interactions, respectively. At smaller k^* , the correlation obtained by the Coulomb + HALQCD elastic agrees with the experimental data much better than the other two, while the Coulomb alone works better around $k^* \simeq 100 - 200$ MeV. Since the inclusion of inelastic contributions estimated by some model makes agreement worse, it will be important to evaluate inelastic contributions directly by the couple channel analysis in the HAL QCD method.

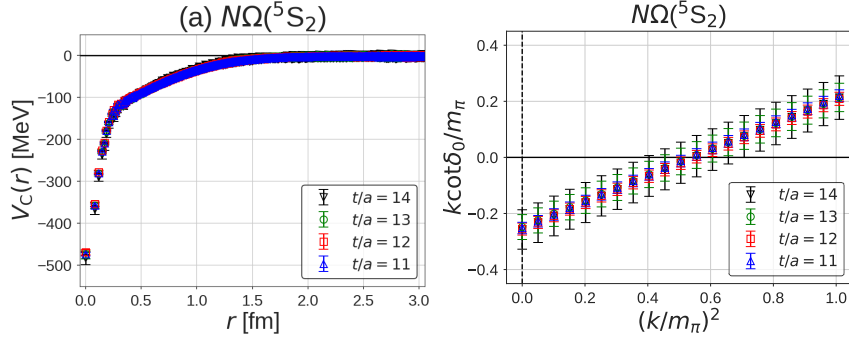


Figure 5: (Left) The $N\Omega$ potential in 5S_2 channel at $t/a = 11$ (blue up triangles), 12 (red squares), 13 (green circles) and 14 (black down triangle). (Right) The $k \cot \delta_0(k)/m_\pi$ as a function of $(k/m_\pi)^2$, where $\delta_0(k)$ is the S -wave scattering phase shift of the $N\Omega({}^5S_2)$ system. Figures taken from Ref. [32].

5. Tetra-quark state T_{cc}

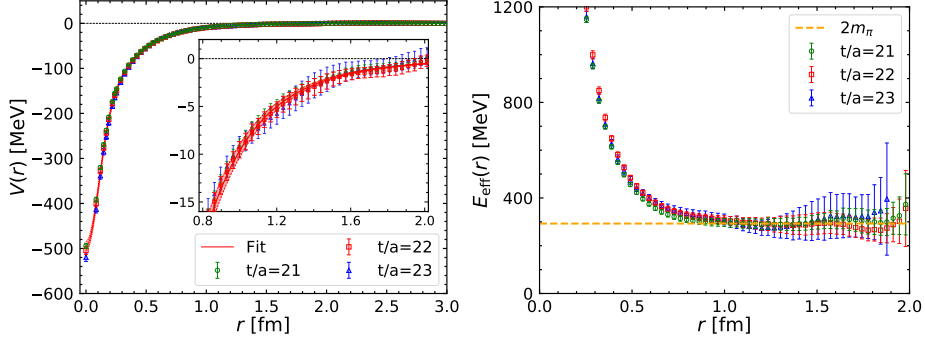


Figure 6: (Left) The D^*D potential $V(r)$ in the $I = 0$ and S -wave channel at $t/a = 21$ (green circles), 22 (red squares) and 23 (blue triangles), while the red band shows the fitted potential with $V_{\text{fit}}(r; m_\pi)$ for $t/a = 22$. (Right) The effective energy $E_{\text{eff}}(r)$ in space as a function of r at three t/a , while the orange dashed line denotes $2m_\pi$ with $m_\pi = 146.4$ MeV. Figures taken from Ref. [36].

A tetra-quark state which contains two heavy (anti-)quarks is a genuine tetra-quark state, since it doesn't couple to ordinary mesons in the the strong interaction due to an absence of pair annihilation channels. Experimentally, LHCb Collaboration reported the observation of the tetra-quark state $T_{cc}(cc\bar{u}\bar{d})$, which appears 360 keV below the $D^{*+}D^0$ thresholds having $(I, J^P) = (0, 1^+)$ [34, 35]. Since the scattering length in the D^*D channel in lattice QCD at heavier pion masses shows the significant pion mass dependence, as seen in Fig. 1 of Ref. [36], the calculation at almost physical pion mass is called for.

There are two channels, $D^0\pi^+D^0$ (3869.25 MeV) and $D^+\pi^0D^0$ (3869.48 MeV), below the $D^{*+}D^0$ threshold (3875.10 MeV) or $D^{*0}D^+$ threshold (3876.51 MeV) in Nature, while, in the isospin symmetric 2+1 flavor lattice QCD at slightly heavier pion mass $m_\pi = 146.4$ MeV, D^*D threshold (3869.3 MeV) is smaller than $D\pi D$ threshold at 3902.8 (3974.3) MeV on $L \rightarrow \infty$ ($L \simeq 8.1$ fm), so that the single D^*D channel analysis is justified.

Fig. 6 (Left) presents the D^*D potential as a function of r , which is attractive at all distances with a long range tail. It turned out that the potential is consistent with (Yukawa)² at large r and is

fitted by two Gaussians plus (Yukawa)²,

$$V_{\text{fit}}(r; m_\pi) = \sum_{i=1,2} a_i e^{-(r/b_i)^2} + a_3 \left(1 - e^{-(r/b_3)^2}\right)^2 \left(\frac{e^{-m_\pi r}}{r}\right)^2, \quad (6)$$

as shown by a red band in the figure. Fig. 6 (Right) gives an effective energy in space, defined by

$$E_{\text{eff}}(r) = -\frac{\ln[V(r)r^2/a_3]}{r} \quad (7)$$

as a function of r , where a_3 is taken from the fitted value in (6). Since $E_{\text{eff}}(r)$ converges to $2m_\pi$ at large r , the 2-pion rather than the 1-pion contribution dominate at long distance. Thus the 1-pion exchange is not a dominant contribution for T_{cc} .

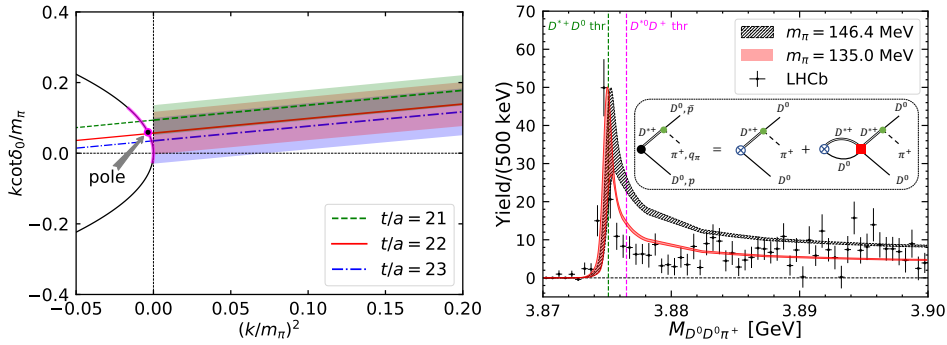


Figure 7: (Left) The $k \cot \delta_0(k)/m_\pi$ for the D^*D scattering in the $I = 0$ and S -wave channel. The intersection of the $k \cot \delta_0(k)/m_\pi$ and the black solid line ($\pm\sqrt{-(k/m_\pi)^2}$) denotes the pole of the scattering amplitude. (Right) The $D^0 D^0 \pi^+$ mass spectrum for theoretical results with $V_{\text{fit}}(r; m_\pi)$ at $m_\pi = 146.4$ MeV (black band) and $m_\pi = 135.0$ MeV (red band) and experimental data by LHCb (black points). Figures taken from Ref. [36].

Fig. 7 (Left) shows $k \cot \delta_0(k)/m_\pi$ as a function of $(k/m_\pi)^2$, where the phases shift $\delta_0(k)$ for the D^*D scattering in the $I = 0$ and S -wave channel are calculated with the fitted potential V_{fit} . This analysis gives an inverse of the scattering length a_0 as $a_0^{-1} [\text{fm}^{-1}] = 0.05(5)_{(-2)}^{(+2)}$. Since the $k \cot \delta_0(k)/m_\pi$ intersects the $+\sqrt{-(k/m_\pi)^2}$ (black solid line), as denoted by “pole” in the figure with magenta line being total errors, there appears one shallow virtual state (not bound state) at $k = i\kappa_{\text{pole}}$ with $\kappa_{\text{pole}} = -8(8)_{(-5)}^{(+3)}$ MeV, equivalently $E_{\text{pole}} = -59_{(-67)}^{(+53)}_{(-2)}$ keV. This virtual pole exists above the left-hand cut for the 1-pion exchange, which appears at $k^2/m_\pi^2 \leq -0.02$ in this lattice setup. The issue on the left-hand cut for T_{cc} and other cases has been discussed in lattice 2024 by the author[37]. See also Refs. [38–40] for the issue.

Table 1: The inverse of the scattering length $1/a_0$, the effective range r_{eff} , the pole position κ_{pole} and E_{pole} at $m_\pi = 146.4$ MeV and 135.0 MeV.

m_π (MeV)	$1/a_0[\text{fm}^{-1}]$	r_{eff} [fm]	κ_{pole} [MeV]	E_{pole} [keV]
146.4	$0.05(5)_{(-2)}^{(+2)}$	$1.12(3)_{(-8)}^{(+3)}$	$-8(8)_{(-5)}^{(+3)}$	$-59_{(-67)}^{(+53)}_{(-2)}$
135.0	$-0.03(4)$	$1.12(3)$	$5(8)$	$-45_{(-78)}^{(+41)}$

We estimate an impact of the small difference in the pion mass on observables between our simulation and Nature, by replacing m_π in $V_{\text{eff}}(r; m_\pi)$ from 146.4 MeV to 135.0 MeV to calculate scattering observables. Results are summarized in Table 1. As seen from signs of $1/a_0$ and κ_{pole} , T_{cc} moves from a shallow virtual state to a shallow bound state by the extrapolation from $m_\pi = 146.4$ MeV to $m_\pi = 135.0$ MeV in terms of the potential. Alternatively, an extrapolation of $1/a_0$ linear in m_π^2 gives $1/a_0 = -0.01(9)$ [fm^{-1}] at $m_\pi = 135.0$ MeV[36]. Thus two extrapolations, $1/a_0[\text{fm}^{-1}] = -0.03(4)$ and $-0.01(9)$, are consistent within errors.

Fig. 7 (Right) shows the $D^0 D^0 \pi^+$ mass spectrum, where black points denote LHCb data while black and red bands represent mass spectra based on $V_{\text{fit}}(r; m_\pi)$ with $m_\pi = 146.4$ MeV and 135.0 MeV, respectively[36]. The potential V_{fit} was employed to estimate the rescattering between D^{*+} and D^0 , denoted by the red circle in the third diagram of the inset in the figure. It seems that the potential extrapolated to $m_\pi = 135$ MeV explains LHCb data better.

6. N - ϕ interaction and the 2-pion tail

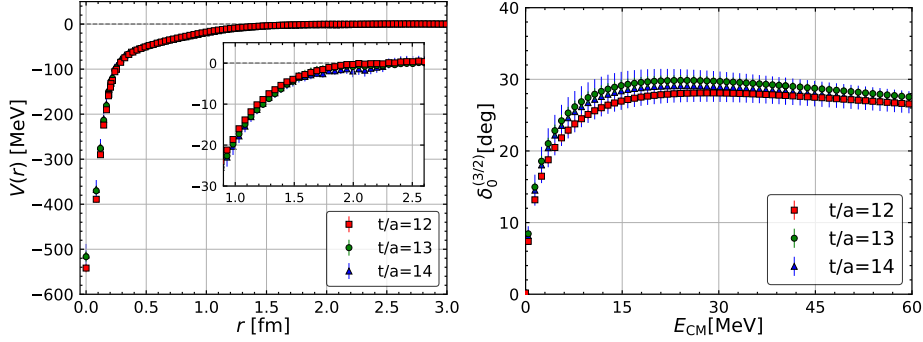


Figure 8: (Left) The $N - \phi$ potential in the ${}^4S_{3/2}$ channel at $t/a = 12$ (red squares), 13 (green circles) and 14 (blue triangle). (Right) The phase shifts $\delta_0^{3/2}$ of the $N - \phi$ scattering in the ${}^4S_{3/2}$ channel, obtained by using $V_{\text{fit}}(r)$ at three t/a . Figures taken from Ref. [41].

The potential between nucleon and ϕ meson in the ${}^4S_{3/2}$ channel was calculated on configurations at $m_\pi \simeq 146$ MeV[41], where there are many channels below the $N\phi({}^4S_{3/2})$ threshold at 2092 MeV. However, contributions from $\Lambda K({}^2D_{3/2})$ at 1665 MeV and $\Sigma K({}^2D_{3/2})$ at 1747 MeV are kinematically suppressed at low energy due to their D -wave nature, and those from $\Lambda\pi K$ (1811 MeV), $\Sigma\pi K$ (1893 MeV) and $\Lambda\pi\pi K$ (1957 MeV) are suppressed due to their small phase spaces. Therefore the single channel analysis of the N - ϕ potential was employed as the first trial.

Fig. 8 (Left) shows the $N - \phi$ potential in the ${}^4S_{3/2}$ channel, which is attractive all distance with a long range tail. As in the case of the D^*D potential, the long range tail is consistent with (Yukawa)², suggesting that the 2-pion exchange appears rather universally. As before, the total potential is fitted by two Gaussians plus (Yukawa)² as

$$V_{\text{fit}}(r; m_\pi) = \sum_{i=1,2} a_i e^{-(r/b_i)^2} + \tilde{a}_3 m_\pi^4 \left(1 - e^{-(r/b_3)^2}\right)^2 \left(\frac{e^{-m_\pi r}}{r}\right)^2, \quad (8)$$

where an extra m_π dependence is introduced by denoting $a_3 = \tilde{a}_3 m_\pi^4$. Fig. 8 (Right) represents the $N - \phi$ scattering phase shift in the ${}^4S_{3/2}$ channel, which leads to the scattering length $a_0^{3/2} =$

$1.43(23)(^{+36}_{-06})$ fm. This value is slightly reduced as $a_0^{3/2} \simeq 1.25$ fm if we use $m_\pi = 138.0$ MeV (isospin averaged physical pion mass) in $V_{\text{fit}}(r; m_\pi)$ instead of $m_\pi = 146.4$ MeV in the simulation.

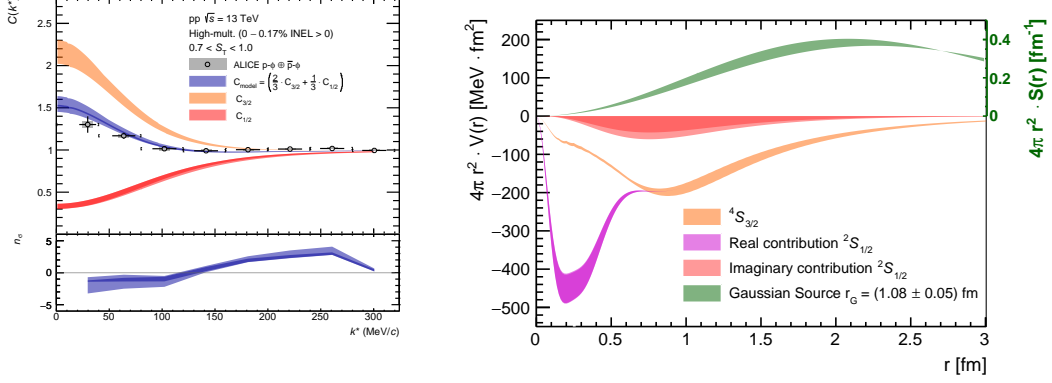


Figure 9: (Left) The $p - \phi$ correlation functions, measured by the ALICE collaboration[43] (gray shaded squares), the $^4S_{3/2}$ contribution $C_{3/2}$ calculated with the lattice potential V_{fit} , the $^2S_{1/2}$ contribution $C_{1/2}$ extracted by the fit (red band) and the total contribution $2C_{3/2}/3 + C_{1/2}/3$ (blue band). The lower panel is the number of standard deviations between ALICE data and the total contribution. (Right) $4\pi r^2 V_{N\phi}^{3/2}(r)$ in the $^4S_{3/2}$ channel as a function of r (orange band), together with the real part (violet band) and the imaginary part (red band) of $4\pi r^2 V^{(1/2)}(r)$ in the $^2S_{1/2}$ channel extracted by the fit. Figures taken from Ref. [42].

Combining the lattice $N\phi(^4S_{3/2})$ potential with the $p - \phi$ correlations measured by the ALICE collaboration, the $N\phi(^2S_{1/2})$ potential was determined[42]. Fig. 9 (Left) shows the $p - \phi$ correlations measured by the ALICE collaboration[43] (gray shaded squares), while the contribution $C_{3/2}$ from the $^4S_{3/2}$ channel is estimated by using the lattice potential V_{fit} (orange band). Since the difference between the experimental data and the $^4S_{3/2}$ contribution represents the contribution $C_{1/2}$ from the $^2S_{1/2}$ channel, the $N\phi(^2S_{1/2})$ potential was determined by assuming the form that

$$V_{N\phi}^{(1/2)}(r) = \beta \sum_{i=1,2} a_i e^{-(r/b_i)^2} + \left(1 - e^{-(r/b_3)^2}\right)^2 \left[\tilde{a}_3 m_\pi^4 \left(\frac{e^{-m_\pi r}}{r}\right)^2 + i\gamma \frac{e^{-2m_K r}}{m_K r^2} \right], \quad (9)$$

where β, γ are fit parameters while a_i, b_i are fixed to values for the $N\phi(^4S_{3/2})$ potential, and the last term with a pure imaginary coefficient represents the 2nd order kaon exchange with the kaon mass m_K . The $^2S_{1/2}$ contribution $C_{1/2}$ (red band) and the total contribution, the weighted average of both $2C_{3/2}/3 + C_{1/2}/3$ (blue band), are also plotted in Fig. 9 (Left). The fit (9) works reasonably well.

Fig. 9 (Right) represents a comparison among potentials in the form of $4\pi r^2 V(r)$ as a function of r , where $V = V_{N\phi}^{(3/2)}$ (orange band), $V = \text{Re}V_{N\phi}^{(1/2)}$ (violet band) and $V = \text{Im}V_{N\phi}^{(1/2)}$ (red band), while the source function $4\pi r^2 S(r)$ is given by the green band. This comparison suggests that the attraction at short distance in the $^2S_{1/2}$ channel, obtained from the fit to the experimental data, is stronger than the one in the $^4S_{3/2}$ channel. The stronger attraction in the $N\phi(^2S_{1/2})$ leads to

$$\text{Re } a_0^{1/2} = -1.47(^{+0.44}_{-0.37})(^{+0.14}_{-0.17}) \text{ fm}, \quad \text{Im } a_0^{1/2} = 0.00(^{+0.26}_{-0.00})(^{+0.15}_{-0.00}) \text{ fm} \quad (10)$$

for the scattering length, which indicates an existence of one $N\phi$ bound state, whose estimated binding energy reads $E_B = 14.7 \sim 56.6$ MeV. For a further conformation in future, it is important to extract $V_{N\phi}^{(1/2)}$ directly by lattice calculations, where the coupled channel analysis among $N\phi$, ΣK and ΛK in ${}^2S_{1/2}$ is required.

7. Summary

There has been a serious ‘‘NN controversy’’ in lattice QCD, that previous studies from the FV method claimed NN systems at heavy pion masses are bound while the HAL QCD method claimed they are unbound. The cross-checks between the FV method and the HAL QCD methods, as well as those within the FV method (and within the HAL QCD method), have been performed and cleared the situation: It is now a consensus among the lattice community that no bound deuteron and dineutron appear at heavy pion masses (at least at the given lattice spacing). The previous claims of bound states of three or more baryons in the FV method[5, 6] are also very likely to be false since the results relied on the same setups and method which lead to incorrect conclusions for two baryon bound states. Accordingly, studies based on the existence of these bound states in the old FV method (e.g., EFT studies, matrix element studies of nuclei) also lost their foundation.

The H-dibaryon seems a ‘‘virtual’’ state near the $N\Xi$ threshold at $m_\pi \simeq 146$ MeV and lattice $N\Xi$ interactions are compared with LHC data obtained by heavy ion collisions. The $N\Omega$ dibaryon is predicted and $p\Omega^-$ interactions are also compared with the LHC data. The tetra-quark state T_{cc} and the $N - \phi$ interaction are investigated also at almost physical pion mass. Both show the 2-pion exchange tail at long distances and results derived from these interactions are compared with experiments. More results at not only $m_\pi \simeq 146$ MeV but also $m_\pi \simeq 137$ MeV[44] will be expected.

References

- [1] M. Luscher, *Two particle states on a torus and their relation to the scattering matrix*, *Nucl. Phys. B* **354** (1991), 531
- [2] N. Ishii, S. Aoki and T. Hatsuda, *The Nuclear Force from Lattice QCD*, *Phys. Rev. Lett.* **99** (2007), 022001 [nucl-th/0611096].
- [3] S. Aoki, T. Hatsuda and N. Ishii, *Theoretical Foundation of the Nuclear Force in QCD and its applications to Central and Tensor Forces in Quenched Lattice QCD Simulations*, *Prog. Theor. Phys.* **123** (2010), 89[0909.5585 [hep-lat]].
- [4] S. Aoki et al. [HAL QCD], *Lattice QCD approach to Nuclear Physics*, *PTEP* **2012** (2012), 01A105 [1206.5088 [hep-lat]].
- [5] T. Yamazaki, K. i. Ishikawa, Y. Kuramashi and A. Ukawa, *Helium nuclei, deuteron and dineutron in 2+1 flavor lattice QCD*, *Phys. Rev. D* **86** (2012), 074514 [1207.4277 [hep-lat]].

- [6] S. R. Beane et al. [NPLQCD], *Light Nuclei and Hypernuclei from Quantum Chromodynamics in the Limit of $SU(3)$ Flavor Symmetry*, *Phys. Rev. D* **87** (2013) 034506 [1206.5219 [hep-lat]].
- [7] T. Yamazaki, K. i. Ishikawa, Y. Kuramashi and A. Ukawa, *Study of quark mass dependence of binding energy for light nuclei in 2+1 flavor lattice QCD*, *Phys. Rev. D* **92** (2015) 014501 [1502.04182 [hep-lat]].
- [8] K. Orginos, A. Parreno, M. J. Savage, S. R. Beane, E. Chang and W. Detmold, *Two nucleon systems at $m_\pi \sim 450$ MeV from lattice QCD*, *Phys. Rev. D* **92** (2015) 114512 [erratum: *Phys. Rev. D* **102** (2020) 039903] [1508.07583 [hep-lat]].
- [9] E. Berkowitz, T. Kurth, A. Nicholson, B. Joo, E. Rinaldi, M. Strother, P. M. Vranas and A. Walker-Loud, *Two-Nucleon Higher Partial-Wave Scattering from Lattice QCD*, *Phys. Lett. B* **765** (2017), 285[1508.00886 [hep-lat]].
- [10] N. Ishii et al. [HAL QCD], *Hadron-hadron interactions from imaginary-time Nambu-Bethe-Salpeter wave function on the lattice*, *Phys. Lett. B* **712** (2012), 437[1203.3642 [hep-lat]].
- [11] T. Inoue et al. [HAL QCD], *Two-Baryon Potentials and H-Dibaryon from 3-flavor Lattice QCD Simulations*, *Nucl. Phys. A* **881** (2012), 28[1112.5926 [hep-lat]].
- [12] https://indico.fnal.gov/event/57249/contributions/271301/attachments/169801/228045/Walker-Loud_NN_LQCD.pdf
- [13] A. Francis, J. R. Green, P. M. Junnarkar, C. Miao, T. D. Rae and H. Wittig, *Lattice QCD study of the H dibaryon using hexaquark and two-baryon interpolators*, *Phys. Rev. D* **99** (2019) 074505 [1805.03966 [hep-lat]].
- [14] B. Hörz, D. Howarth, E. Rinaldi, A. Hanlon, C. C. Chang, C. Körber, E. Berkowitz, J. Bulava, M. A. Clark and W. T. Lee, et al. *Two-nucleon S-wave interactions at the $SU(3)$ flavor-symmetric point with $m_{ud} \simeq m_s^{\text{phys}}$: A first lattice QCD calculation with the stochastic Laplacian Heaviside method*, *Phys. Rev. C* **103** (2021) 014003 [2009.11825 [hep-lat]].
- [15] S. Amarasinghe, R. Baghdadi, Z. Davoudi, W. Detmold, M. Illa, A. Parreno, A. V. Pochinsky, P. E. Shanahan and M. L. Wagman, *Variational study of two-nucleon systems with lattice QCD*, *Phys. Rev. D* **107** (2023) 094508 [erratum: *Phys. Rev. D* **110** (2024) 119904] [2108.10835 [hep-lat]].
- [16] T. Iritani, T. Doi, S. Aoki, S. Gongyo, T. Hatsuda, Y. Ikeda, T. Inoue, N. Ishii, K. Murano and H. Nemura, et al. *Mirage in Temporal Correlation functions for Baryon-Baryon Interactions in Lattice QCD*, *JHEP* **10** (2016), 101 [1607.06371 [hep-lat]].

- [17] T. Iritani, S. Aoki, T. Doi, T. Hatsuda, Y. Ikeda, T. Inoue, N. Ishii, H. Nemura and K. Sasaki, *Are two nucleons bound in lattice QCD for heavy quark masses? Consistency check with Lüscher's finite volume formula*, *Phys. Rev. D* **96** (2017)034521 [1703.07210 [hep-lat]].
- [18] T. Iritani et al. [HAL QCD], *Consistency between Lüscher's finite volume method and HAL QCD method for two-baryon systems in lattice QCD*, *JHEP* **03** (2019), 007 [1812.08539 [hep-lat]].
- [19] <https://indico.hiskp.uni-bonn.de/event/40/contributions/795/attachments/564/964/Lattice2022.pdf>
- [20] F. Winter, W. Detmold, A. S. Gambhir, K. Orginos, M. J. Savage, P. E. Shanahan and M. L. Wagman, *First lattice QCD study of the gluonic structure of light nuclei*, *Phys. Rev. D* **96** (2017)094512 [1709.00395 [hep-lat]].
- [21] J. R. Green, *Status of two-baryon scattering in lattice QCD*, [tt 2502.15546 [hep-lat]].
- [22] <https://agenda.infn.it/event/7897/contributions/70535/attachments/51374/60696/CD15SilasBeane.pdf>
- [23] N. Barnea, L. Contessi, D. Gazit, F. Pederiva and U. van Kolck, *Effective Field Theory for Lattice Nuclei*, *Phys. Rev. Lett.* **114** (2015)052501 [1311.4966 [nucl-th]].
- [24] V. Baru, E. Epelbaum, A. A. Filin and J. Gegelia, *Low-energy theorems for nucleon-nucleon scattering at unphysical pion masses*, *Phys. Rev. C* **92** (2015)014001 [1504.07852 [nucl-th]].
- [25] V. Baru, E. Epelbaum and A. A. Filin, *Low-energy theorems for nucleon-nucleon scattering at $M_\pi = 450$ MeV*, *Phys. Rev. C* **94** (2016) no.1, 014001 [1604.02551 [nucl-th]].
- [26] K. I. Ishikawa et al. [PACS], *2+1 Flavor QCD Simulation on a 96^4 Lattice*, *PoS LATTICE2015* (2016), 075 [1511.09222 [hep-lat]].
- [27] T. Inoue et al. [HAL QCD], *Bound H-dibaryon in Flavor SU(3) Limit of Lattice QCD*, *Phys. Rev. Lett.* **106** (2011), 162002 [1012.5928 [hep-lat]].
- [28] T. Inoue et al. [HAL QCD], *Baryon-Baryon Interactions in the Flavor SU(3) Limit from Full QCD Simulations on the Lattice*, *Prog. Theor. Phys.* **124** (2010), 591[1007.3559 [hep-lat]].
- [29] K. Sasaki et al. [HAL QCD], *$\Lambda\Lambda$ and $N\Xi$ interactions from lattice QCD near the physical point*, *Nucl. Phys. A* **998** (2020), 121737 [1912.08630 [hep-lat]].

- [30] S. Acharya et al. [ALICE], *First Observation of an Attractive Interaction between a Proton and a Cascade Baryon*, *Phys. Rev. Lett.* **123** (2019)112002 [1904.12198 [nucl-ex]].
- [31] A. Collaboration et al. [ALICE], *Unveiling the strong interaction among hadrons at the LHC*, *Nature* **588** (2020), 232[erratum: *Nature* **590** (2021), E13] [2005.11495 [nucl-ex]].
- [32] T. Iritani et al. [HAL QCD], *$N\Omega$ dibaryon from lattice QCD near the physical point*, *Phys. Lett. B* **792** (2019), 284[1810.03416 [hep-lat]].
- [33] F. Etminan et al. [HAL QCD], *Spin-2 $N\Omega$ dibaryon from Lattice QCD*, *Nucl. Phys. A* **928** (2014), 89[1403.7284 [hep-lat]].
- [34] R. Aaij et al. [LHCb], *Observation of an exotic narrow doubly charmed tetraquark*, *Nature Phys.* **18** (2022) 751 [2109.01038].
- [35] R. Aaij et al. [LHCb], *Study of the doubly charmed tetraquark T_{cc}^+* , *Nature Commun.* **13** (2022) 3351 [2109.01056].
- [36] Y. Lyu, S. Aoki, T. Doi, T. Hatsuda, Y. Ikeda and J. Meng, *Doubly Charmed Tetraquark T_{cc}^+ from Lattice QCD near Physical Point*, *Phys. Rev. Lett.* **131** (2023) 161901 [2302.04505].
- [37] S. Aoki, T. Doi and Y. Lyu, *Left-hand cut and the HAL QCD method*, *PoS LATTICE2024* (2025), 089 [2501.16804 [hep-lat]].
- [38] M. L. Du, A. Filin, V. Baru, X. K. Dong, E. Epelbaum, F. K. Guo, C. Hanhart, A. Nefediev, J. Nieves and Q. Wang, *Role of Left-Hand Cut Contributions on Pole Extractions from Lattice Data: Case Study for $T_{cc}(3875)^+$* , *Phys. Rev. Lett.* **131** (2023) 131903 [2303.09441].
- [39] L. Meng, V. Baru, E. Epelbaum, A. A. Filin and A. M. Gasparyan, *Solving the left-hand cut problem in lattice QCD: $T_{cc}(3875)^+$ from finite volume energy levels*, *Phys. Rev. D* **109** (2024) L071506 [2312.01930].
- [40] S. Collins, A. Nefediev, M. Padmanath and S. Prelovsek, *Toward the quark mass dependence of T_{cc}^+ from lattice QCD*, *Phys. Rev. D* **109** (2024) 094509 [2402.14715].
- [41] Y. Lyu, T. Doi, T. Hatsuda, Y. Ikeda, J. Meng, K. Sasaki and T. Sugiura, *Attractive N - ϕ interaction and two-pion tail from lattice QCD near physical point*, *Phys. Rev. D* **106** (2022)074507 [2205.10544 [hep-lat]].
- [42] E. Chizzali, Y. Kamiya, R. Del Grande, T. Doi, L. Fabbietti, T. Hatsuda and Y. Lyu, *Indication of a p - ϕ bound state from a correlation function analysis*, *Phys. Lett. B* **848** (2024), 138358 [2212.12690 [nucl-ex]].

- [43] S. Acharya et al. [ALICE], *Experimental Evidence for an Attractive p - ϕ Interaction*, *Phys. Rev. Lett.* **127** (2021)172301 [2105.05578 [nucl-ex]].
- [44] T. Aoyama et al. [HAL QCD], *Scale setting and hadronic properties in the light quark sector with (2+1)-flavor Wilson fermions at the physical point*, *Phys. Rev. D* **110** (2024) no.9, 094502 [2406.16665 [hep-lat]].